



Breakdown of clonal cooperative architecture in multispecies biofilms and the spatial ecology of predation

Benjamin R. Wucher^a, James B. Winans^a, Mennat Elsayed^b, Daniel E. Kadouri^b , and Carey D. Nadell^{a,1}

Edited by Joan Strassmann, Washington University in St. Louis, St. Louis, MO; received July 22, 2022; accepted November 6, 2022

Biofilm formation, including adherence to surfaces and secretion of extracellular matrix, is common in the microbial world, but we often do not know how interaction at the cellular spatial scale translates to higher-order biofilm community ecology. Here we explore an especially understudied element of biofilm ecology, namely predation by the bacterium *Bdellovibrio bacteriovorus*. This predator can kill and consume many different Gram-negative bacteria, including *Vibrio cholerae* and *Escherichia coli*. *V. cholerae* can protect itself from predation within densely packed biofilm structures that it creates, whereas *E. coli* biofilms are highly susceptible to *B. bacteriovorus*. We explore how predator–prey dynamics change when *V. cholerae* and *E. coli* are growing in biofilms together. We find that in dual-species prey biofilms, *E. coli* survival under *B. bacteriovorus* predation increases, whereas *V. cholerae* survival decreases. *E. coli* benefits from predator protection when it becomes embedded within expanding groups of highly packed *V. cholerae*. But we also find that the ordered, highly packed, and clonal biofilm structure of *V. cholerae* can be disrupted if *V. cholerae* cells are directly adjacent to *E. coli* cells at the start of biofilm growth. When this occurs, the two species become intermixed, and the resulting disordered cell groups do not block predator entry. Because biofilm cell group structure depends on initial cell distributions at the start of prey biofilm growth, the surface colonization dynamics have a dramatic impact on the eventual multispecies biofilm architecture, which in turn determines to what extent both species survive exposure to *B. bacteriovorus*.

biofilm | matrix | predator-prey | architecture | cooperation

Most organisms do not naturally live in isolated monocultures but rather in communities composed of many species, and microbes are no exception (1–4). Bacterial communities are present ubiquitously including sinking detritus particles in aquatic environments, deep-sea hydrothermal vents, rhizosphere habitats, animal digestive tracts, fouling surfaces across human industry, and many types of chronic infections (5–19). In many of these contexts, surface attachment and growth in large cell groups, or biofilm formation, are important strategies for sequestering limited space and nutrients, as well as protecting against common biotic and abiotic threats (20–25). Biofilms are small-scale ecosystems encased in a wide range of secreted polymeric substances that control cell–cell and cell–surface engagement (26–32). The benefits of biofilm formation have been examined in many contexts, showing their capacity for public goods sequestration, exclusion of newly arriving competitors, predation protection, and antibiotic tolerance (33–37). The precise functions of biofilm formation vary across species, as do the multicellular architectures that emerge from the combination of cell growth, matrix secretion, and environmental feedbacks (23, 27, 29, 38–46). In what few cases have been examined, multispecies biofilms create structures that may be distinct from those found in single species biofilms of the community constituents in isolation (47–49). Understanding the connections between biofilm architecture and microbial community ecology at different scales remains an important area for ongoing work on numerous topics, including cross-feeding relationships, diffusible and contact-mediated toxin antagonism, resilience against antibiotics in therapeutic contexts, industrial and medical surface degradation, and others (50–56).

Predation within biofilms is a broad subclass of microbial ecology that has received relatively little attention with high-resolution imaging and analysis. While many predators, such as phages, can usually attack only a small number of prey species, the ubiquitous predator *Bdellovibrio bacteriovorus* can be considered a generalist (36, 57–60). It is not known to rely on a specific receptor for cell entry and can prey on a variety of proteobacteria (8, 59, 61–63). However, the extent of its predation on biofilm-dwelling target cells appears to vary widely between prey species, and the mechanisms underlying this variability remain mostly unknown.

Studies using macroscopic measurement techniques have reported the susceptibility of several biofilm-producing species to *B. bacteriovorus* predation (57). For example,

Significance

Bacteria live in multispecies, spatially structured communities ubiquitously in the natural world. These communities, or biofilms, have a strong impact on microbial ecology, but we often do not know how cellular scale interactions determine overall biofilm structure and community dynamics. Here we explore this problem in the context of predator–prey interaction, with two prey species—*Vibrio cholerae* and *Escherichia coli*—being attacked by the bacterial predator *Bdellovibrio bacteriovorus*. We find that when *V. cholerae* and *E. coli* grow together in biofilms, the architectures that they produce change in ways that cannot be predicted from looking at each prey species alone, and that these changes in cell group structure impact the community dynamics of predator–prey interaction in biofilms.

Author affiliations: ^aDepartment of Biological Sciences, Dartmouth, Hanover, NH 03755; and ^bDepartment of Oral Biology, Rutgers School of Dental Medicine, Newark, NJ 07101

Author contributions: B.R.W., J.B.W., and C.D.N. designed research; B.R.W. and J.B.W. performed research; B.R.W., M.E., D.E.K., and C.D.N. contributed new reagents/analytic tools; B.R.W., J.B.W., and C.D.N. analyzed data; C.D.N. supervised and acquired funding for the project; and B.R.W. and C.D.N. wrote the paper.

The authors declare no competing interest.

This article is a PNAS Direct Submission.

Copyright © 2023 the Author(s). Published by PNAS. This article is distributed under Creative Commons Attribution-NonCommercial-NoDerivatives License 4.0 (CC BY-NC-ND).

¹To whom correspondence may be addressed. Email: carey.d.nadell@dartmouth.edu.

This article contains supporting information online at <https://www.pnas.org/lookup/suppl/doi:10.1073/pnas.2212650120/-DCSupplemental>.

Published February 2, 2023.

Escherichia coli and *Pseudomonas fluorescens* can be largely consumed by *B. bacteriovorus* in laboratory biofilm culture (36). We recently documented a different outcome in *Vibrio cholerae* biofilms, which can protect themselves from predator exposure via their highly packed cell arrangements that occur after the prey cell groups grow beyond several hundred cells (35). Given that we have examples of prey species whose biofilm structure protects them from *B. bacteriovorus* predation, and other prey whose biofilms confer little protection, we were curious as to what would happen to predator–prey dynamics in multispecies prey biofilm contexts. How often and to what extent does the cellular architecture of the two species in co-culture depart from what is normally observed in monoculture? How do any of these changes influence the susceptibility of different prey species to *Bdellovibrio* predation and overall predator–prey population dynamics?

We chose two proteobacteria—*V. cholerae* and *E. coli*—to study these questions. Both species have been isolated from biofilms in the same environments in proximity to humans, and they can coinfect hosts (64–69). Their respective biofilm formation mechanics have also been very well characterized. *V. cholerae* forms dense cell groups whose structure depends on the matrix proteins RbmA, RbmC, and Bap1, as well as vibrio polysaccharide (VPS) (27, 28, 40, 70–72). This highly packed cell group architecture is critical for protection from phages and from *B. bacteriovorus* (35, 37). The cell packing required for predator protection does not occur immediately as biofilm growth begins, though, leaving smaller *V. cholerae* cell groups open to predation. *E. coli* by contrast forms biofilms with many different matrix components including cellulose, polyglycolic acid, colanic acid, Type 1 fimbriae, flagellar filaments, and curli fiber proteins (73). *E. coli* matrix architecture and curli protein, in particular, have been shown to confer protection against phage exposure, but other prior work has indicated that *E. coli* biofilms are not protected from *B. bacteriovorus* (57, 74). Here we use single-cell resolution microscopy to examine the structure of these two prey species in monoculture and dual-culture biofilms, finding that the multispecies context causes unexpected changes in biofilm architecture that in turn alter predator–prey interaction and the overall population dynamics.

Results

Predation in Dual-Species Prey Biofilms has Opposite Fitness Effects for *E. coli* and *V. cholerae*. We engineered *V. cholerae* N16961, *E. coli* AR3110, and *B. bacteriovorus* 109J to constitutively produce the fluorescent proteins mKate2, mKO-κ, and GFP, respectively, so that they could be distinguished by live confocal microscopy. N16961 is naturally repressed for Type VI Secretion System activity in many conditions, and it does not kill *E. coli* via this mechanism in our experiments (75–77). Overnight cultures of the two prey species were both normalized to OD₆₀₀ = 1.0 before inoculating them at a 1:1 ratio into poly-dimethylsiloxane microfluidic flow devices bonded to coverslip glass (see *Materials and Methods*). In parallel, we performed monoculture experiments in which *V. cholerae* and *E. coli* were introduced to chambers on their own. Cells were allowed to colonize the underlying glass surface in stationary conditions for 1 h, after which M9 minimal media with 0.5% glucose was introduced into the chambers at 0.2 μL/min (average flow velocity = 90 μm/s). After 48 h of growth in co-culture, groups with varying composition of both species could be found distributed throughout the chambers (*SI Appendix*, Fig. S1A), and prior to exposure to *B. bacteriovorus*, the two prey species equilibrated at frequencies of ~90% *V. cholerae* and ~10% *E. coli* (Fig. 1 and *SI Appendix*, Fig. S1A). Following 48 h of prey biofilm growth, we introduced *B. bacteriovorus* under continuous

flow for 1 h, followed by a return to influx of sterile M9 media for both the dual-culture chambers and the monoculture controls. When exposed to *B. bacteriovorus* in a mono-species context, *V. cholerae* survives within cell groups that have reached high cell packing, as we have shown previously (35). 48 h following predator exposure, monoculture *V. cholerae* biofilms maintain net positive growth (Fig. 1 A and B). By contrast, and consistent with prior reports, *E. coli* biofilms in monoculture exhibit little survival in the presence of *B. bacteriovorus*, with viable prey biomass (i.e., *E. coli* cells without *B. bacteriovorus* inside or attached to them) falling nearly to zero 48 h after predator introduction (Fig. 1 A and B and *SI Appendix*, Fig. S1B) (36).

If *B. bacteriovorus* predaes *V. cholerae* and *E. coli* independently of one another in dual prey species biofilms, we would expect residual *V. cholerae* biomass and elimination of most *E. coli* subpopulations, as seen in the prey monoculture experiments above. However, examining the population dynamics quantitatively, we found a significant increase in *E. coli* survival and a modest decrease in *V. cholerae* survival following predator introduction in the dual-species condition relative to the single species controls (Fig. 1). These results imply interactions between *V. cholerae*, *E. coli*, and *B. bacteriovorus*, which alter prey population dynamics in a manner that the mono-species controls cannot predict. Below we explore why *E. coli* fares better in dual-species biofilms against predator exposure, and why *V. cholerae* fares worse, relative to their respective single species prey conditions.

***E. coli* gains Protection from Predator Exposure while Embedded within *V. cholerae* Cell Groups.** Prior to introduction of *B. bacteriovorus* predators, we noticed that the spatial distributions of *V. cholerae* and *E. coli* in dual-culture prey biofilms were heterogeneous on scales of 10 to 100 μm, and in some locations, there were groups of *E. coli* cells that had been enveloped by along the basal layers of expanding colonies of highly packed *V. cholerae*. 48 h following introduction of predators, most surviving *E. coli* were those embedded along the bottom of packed *V. cholerae* biofilms in this manner (Fig. 2A and *SI Appendix*, Figs. S2 and S4D). As previously documented, *V. cholerae* biofilm clusters reach a cell packing threshold that blocks predator entry and allows the interior cells to survive (35). *E. coli* cells enveloped within *V. cholerae* groups that have reached this threshold appear to gain the predation protection conferred by *V. cholerae* biofilm structure. To assess this point in more detail, we quantified the extent of *E. coli* predation and *V. cholerae* fluorescence in proximity to *E. coli* in these images; *E. coli* with high *V. cholerae* fluorescence in close proximity clearly also experienced the least predation (Fig. 2 B and C; this result is clarified with further quantitative detail in the next section). Additionally, protection of *E. coli* within *V. cholerae* cell groups was dependent on the high-density structure that wild-type *V. cholerae* creates. When the experiment was repeated with a mutant strain of *V. cholerae* that cannot produce RbmA—a matrix component required for the tight cell packing found in mature biofilms—*B. bacteriovorus* could freely enter and access both *V. cholerae* and *E. coli* (*SI Appendix*, Fig. S3 A and B). In this case, almost all cells of both species were killed off by the predators (*SI Appendix*, Fig. S3 C and D). In a parallel study illustrating the generality of these results, we show that *E. coli* embedded within expanding *V. cholerae* biofilm clusters are also protected from exposure to the obligate lytic phage T7 and temperate phage λ in a manner dependent on the high-packing structure of *V. cholerae* biofilms (78).

Although *E. coli* cells embedded within *V. cholerae* biofilms gain predator protection, it was not clear if they remain viable, or if they are able to subsequently disperse to colonize downstream locations. If not, then the protection *E. coli* gains from *B. bacteriovorus*

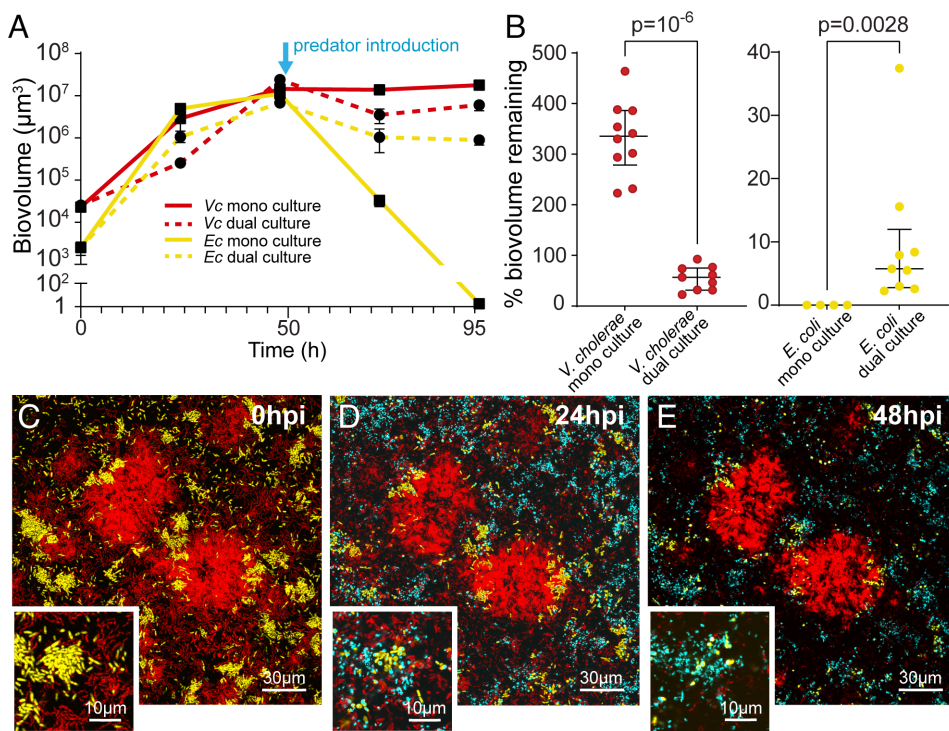


Fig. 1. Population dynamics in monoculture and dual-culture biofilms of *V. cholerae* (red) and *E. coli* (yellow) undergoing predation by *B. bacteriovorus* (cyan). Biofilms of *V. cholerae* and *E. coli* were grown for 48 h prior to *B. bacteriovorus* predator exposure. (A) Population dynamics of each prey species in monoculture and dual-culture biofilm growth ($n = 4$). (B) Percent change in prey biovolume, a direct proxy for population size, 48 h after predator introduction relative to just prior to predator introduction, both in single species prey biofilm controls and dual-species prey co-culture biofilm conditions. (*V. cholerae* monoculture $n = 10$; *V. cholerae* dual culture $n = 9$; *E. coli* monoculture $n = 4$; *E. coli* dual culture $n = 9$). Pairwise comparisons were performed by Mann–Whitney *U* tests. (C–E) Representative images of dual-culture biofilms at (C) 48 h after initial prey inoculation (just prior to predator introduction; "hpi" denotes "hours post-introduction" of predators), (D) 24 h post-introduction of predators, and (E) 48 h post-introduction of predators. Inset frames show regions with details of predators entering host cells and forming rounded bdelloplasts, indicating active predation. Images are single optical sections just above the glass substratum, showing the bottom layers of the biofilms.

exposure within *V. cholerae* cell groups would not necessarily translate to meaningful fitness gains on longer timescales. We explored this question by inducing a disturbance regimen following *B. bacteriovorus* predation of co-culture prey biofilms, allowing the *V. cholerae* and *E. coli* to colonize new microfluidic devices from the effluent exiting the initial chambers. We could show that almost

all *E. coli* outside the periphery of highly packed *V. cholerae* colonies were killed by *B. bacteriovorus* exposure, and that the remaining *E. coli* that were protected while embedded within *V. cholerae* colonies remained viable. When these surviving *E. coli* cells were dislodged by disturbance, they could successfully colonize new locations downstream (SI Appendix, Fig. S4).

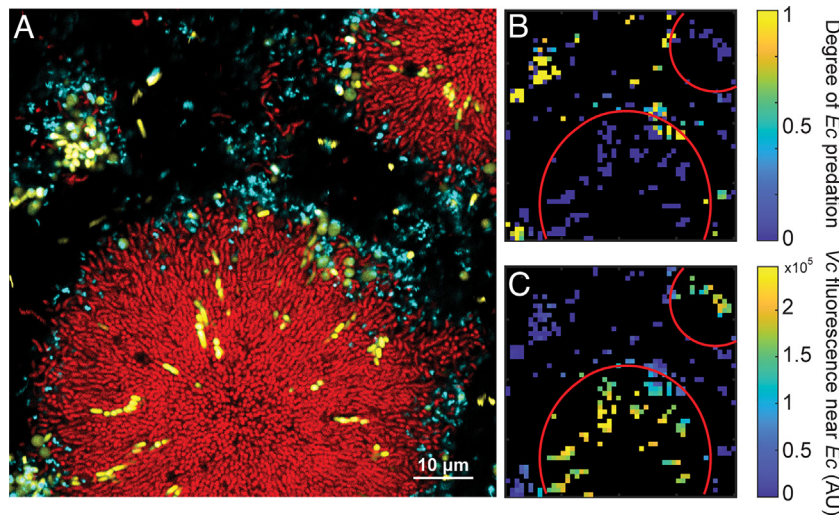


Fig. 2. *E. coli* (yellow) enveloped within highly packed *V. cholerae* biofilms (red) can be protected from *B. bacteriovorus* (cyan) exposure. (A) Representative image demonstrating the ability of highly packed *V. cholerae* biofilms to protect *E. coli* biomass from access by *B. bacteriovorus*. The image is a single optical section just above the glass substratum. (B) Heatmap of the degree of predation on *E. coli*, quantifying raw data from panel A. Red circles denote boundaries of highly packed *V. cholerae* cell groups. (C) Heatmap of *V. cholerae* fluorescence within 5 μm of each unit of segmented biovolume of *E. coli* from panel A.

The predation protection gained by *E. coli* cell groups embedded within highly packed *V. cholerae* biofilm clusters explains the increase in *E. coli* survivorship that we originally observed in dual culture. We note however that the *V. cholerae* cells within these cell groups are also protected from *B. bacteriovorus* predation (Fig. 2), so the results so far do not yet explain why *V. cholerae* survivorship declines in co-culture with *E. coli* under predation pressure.

Co-Culture with *E. coli* Can Lead to Breakdown of *V. cholerae* Biofilm Architecture.

In the previous section, we made note of highly packed *V. cholerae* biofilms into which *E. coli* had become embedded and gained protection from *B. bacteriovorus* exposure. These colonies appear to behave in much the same way as mono-species *V. cholerae* biofilms, as they contain large continuous groups of *V. cholerae* in their ordered radial alignment and tight packing, albeit with pockets of *E. coli* along the glass substratum included as well (Fig. 3 A and B). This growth pattern was not the only kind that emerged in prey co-culture experiments, however: There was a second, qualitatively distinct colony architecture in which *V. cholerae* and *E. coli* were homogenously mixed together (Fig. 3 A and C). These colonies were disordered in comparison with the radial alignment in ordered *V. cholerae* cell groups, with visibly reduced cell packing density. *B. bacteriovorus* could enter throughout these disordered cell groups, gaining access to and killing most *V. cholerae* and *E. coli* cells within them (Fig. 3 A and C).

To study the differences between the ordered and disordered colony structure in more detail, we isolated examples of each for further analysis (Fig. 3 B and C). The relative abundance of *V. cholerae* looked to be somewhat lower in disordered colonies (Fig. 3 B and C, see also next section for quantitative detail). The combined cell packing of the two species together was indeed reduced in disordered colonies (Fig. 3 D), falling below the threshold necessary for predation protection in ordered *V. cholerae* cell groups (35). An alternative but not mutually exclusive factor for predation susceptibility for *V. cholerae* could be abundance of *E. coli* in their immediate vicinity. However, measurements of the relationship between *V. cholerae* predation and local abundance of *E. coli* in the two colony types clearly show that overall colony structure is the dominant factor controlling the extent of predation by *B. bacteriovorus* (Fig. 3 E). A similar reciprocal analysis of *E. coli* predation as a function of colony type and local abundance of *V. cholerae* gave the same outcome (SI Appendix, Fig. S5). The shift in architecture between ordered and disordered cell groups also appeared to be driven entirely by the loss of *V. cholerae*'s ability to produce highly packed clusters, as it normally does on its own. Examining the cell packing of groups formed after 48 h supports this interpretation, as *V. cholerae* within-species cell packing with respect to itself (by contrast with joint cell packing of the two species together noted in Fig. 3 D) shifted between ordered versus disordered biofilm types (Fig. 3 F). *E. coli* within-species cell packing, on the other hand, was not statistically different in ordered versus

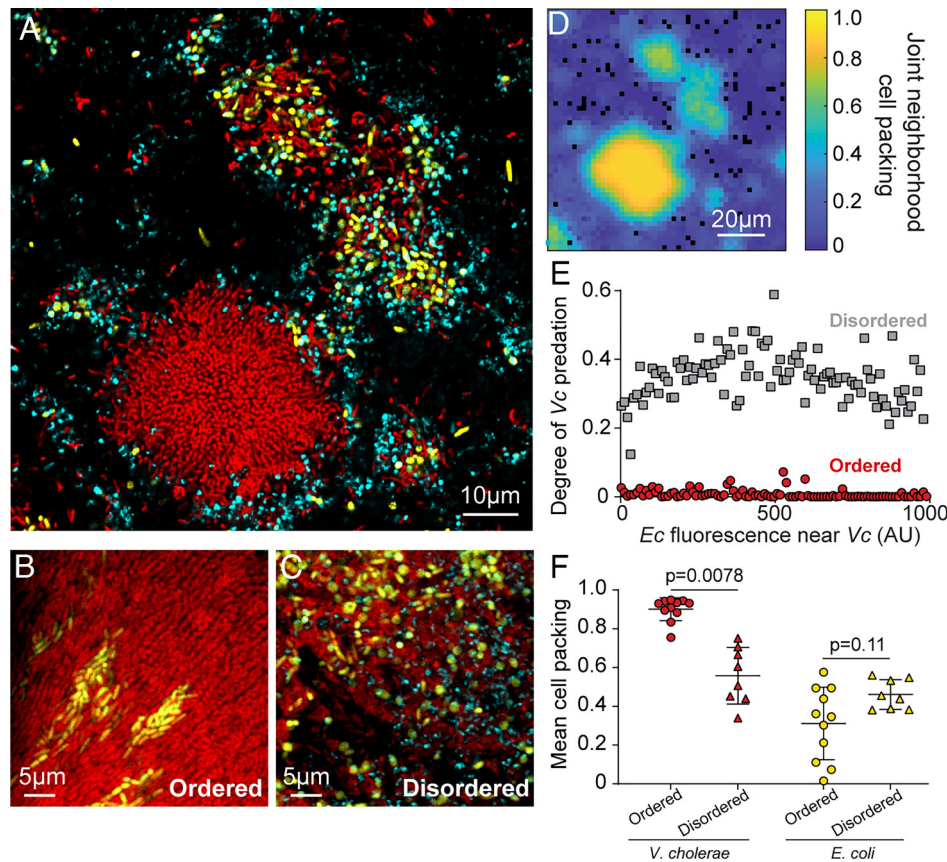


Fig. 3. *V. cholerae* (red) and *E. coli* (yellow) exhibit two distinct joint biofilm morphologies in co-culture that strongly affect *B. bacteriovorus* (cyan) predation susceptibility. (A) Representative image of both biofilm dual-species cell group types, which can occur in close proximity. The structure we term "ordered" more closely resembles the architecture *V. cholerae* produces on its own and is shown on the lower left in this image. The novel, well-mixed structure, which we term "disordered," is shown on the upper right. (B and C) Additional higher magnification images detailing the architecture of ordered and disordered colony morphologies. (D) Heatmap of the combined two-species neighborhood cell packing values for the image in panel A. (E) Scatterplot of the degree of predation on *V. cholerae* as a function of the fluorescence of *E. coli* in proximity to *V. cholerae* biomass. The data are split according to whether they are from ordered architecture colonies ($n = 11$), or disordered colonies ($n = 8$). (F) Within-species cell packing for *V. cholerae* (red) and *E. coli* (yellow) in 48 h incubated cell groups of each structure type (ordered $n = 11$; disordered $n = 8$). Pairwise comparisons were performed by Wilcoxon signed ranks tests.

disordered cell groups (Fig. 3*F*). On longer timescales, it should be noted, *E. coli* cell groups that have been enveloped within ordered *V. cholerae* colonies can also be driven to high within-species cell packing by the confinement imposed by *V. cholerae* biofilm architecture (78).

Our results thus far indicate that in mixed prey biofilms of *V. cholerae* and *E. coli*, a fraction of the *E. coli* along the basal surface becomes engulfed within *V. cholerae* cell groups with ordered high-packing structure that protects both species from *B. bacteriovorus*. This observation explains the improvement in *E. coli* predation survival in dual culture relative to monoculture biofilms. On the other hand, a fraction of the *V. cholerae* population becomes entangled with *E. coli* in well-mixed colonies that fail to develop *V. cholerae*'s normal packing structure, instead growing into disordered, loosely assembled groups that are fully susceptible to predation. This observation clarifies why *V. cholerae* predation protection declines in biofilm co-culture with *E. coli* on a population-wide scale.

Mixed Species Cell Groups Follow Distinct Trajectories Depending on Surface Colonization Conditions. To better understand how the highly packed versus disordered dual-species colonies originate, we ran new experiments tracking biofilm growth at 1 h intervals from the initial stages of surface colonization to clusters containing hundreds of cells at 48 h. Examples of the two cell group types were found by visual inspection at 48 h and then traced back to their initial conditions corresponding to 9 h after the start of incubation (Fig. 4 *A* and *C*). On larger spatial scales than shown in Fig. 4, both types of colony morphology could be found in close proximity (Fig. 3*A* and *SI Appendix*, Fig. S6). The two colony types could be reliably distinguished by their combined cell packing, which was systematically lower in the core regions of disordered colonies (Fig. 4 *B* and *D*, see below for temporally resolved detail). The two colony structures were also consistently different in total biovolume and species composition at 48 h, with ordered high-packing cell groups growing to larger population sizes and containing higher relative abundance of *V. cholerae* compared to *E. coli* (Fig. 4 *E* and *F*).

Though the two biofilm architectures could be quantitatively separated in several respects after they had grown to several hundred cells in size, the mean distance between *V. cholerae* and *E. coli* cells was the only factor we could discern at early time points that clearly differentiated cell groups that would later become ordered, highly packed biofilms versus disordered cell groups (Fig. 4*G* and *SI Appendix*, Fig. S7). The two cell group types in fact begin and remain on different trajectories with respect to *V. cholerae*-*E. coli* distance across all replicate colony time series acquisitions. *V. cholerae* that produced ordered, highly packed architecture were on average 8 μm away from the nearest *E. coli* cell at early time points, while those that became disordered clusters were only 1 μm from the nearest *E. coli* cell at early time points (Fig. 4 *G* and *H*). This observation suggests that the colonization conditions at the beginning of biofilm growth, as surface-attached cells are just starting to divide in place, are crucial for the eventual consolidation of *V. cholerae* packing architecture.

Reviewing the data obtained from time series of the two dual-species colony structures, we also noted an important transition that occurs in ordered high-packing *V. cholerae* cell groups. In our culture conditions at ~19 to 26 h, a core region of highly packed *V. cholerae* cells is nucleated (Fig. 4*J*). This process creates a secondary front of structural consolidation that lags behind the outermost, less densely packed growth front that represents the interface between the growing colony and the surrounding liquid medium (Fig. 4*B*). This secondary front bounding the

central core biofilm region has been observed previously (28, 29, 79, 80), and it corresponds to the portion of the cell group with sufficiently high cell density to provide predator protection (35). In disordered colonies containing well-mixed *V. cholerae* and *E. coli*, the nucleation of this high-density core never occurs. This difference between the two cell group types can be tracked quantitatively via the cell packing of the inner core of each (Fig. 4*J*). In ordered colonies, once the highly packed core was initiated, it was stable over time, and interruption of this core nucleation process only occurred if *V. cholerae* and *E. coli* cells happened to begin growing in close proximity from the start of biofilm formation. Allowing *V. cholerae* to grow on its own for 48 h, followed by invasion of *E. coli* into the biofilm environment, never led to any observable disruption of highly packed *V. cholerae* groups. Introduced planktonic *E. coli* cells could not invade *V. cholerae* biofilms and were completely susceptible to predation if *B. bacteriovorus* was later added to the system (*SI Appendix*, Fig. S8).

Our results here highlight critical points for the production of *V. cholerae* biofilm structure with its characteristic packing and cell alignment architecture (27–29, 34, 79, 80), which in turn are necessary for protection from *B. bacteriovorus* (35). If *V. cholerae* cells are sufficiently isolated during early biofilm formation, they can grow, divide, and secrete biofilm matrix components that effectively coordinate their normal architecture. However, if *V. cholerae* cells are too close to *E. coli* at the start of biofilm formation, the two species become entangled in the process of growth and division in a manner that interrupts the longer-term production of cell group architecture that *V. cholerae* normally produces on its own. The disruption of the structure that *V. cholerae* typically produces suggests that if *E. coli* is in close enough proximity at early stages of growth, *V. cholerae* either does not produce biofilm matrix normally, or it does produce matrix, but with a disruption of the cell-cell orientation and matrix localization that *V. cholerae* would obtain on its own.

To begin parsing these possibilities, we performed additional biofilm co-culture experiments in which *V. cholerae* produced a FLAG-labeled version of one of its primary matrix proteins RbmA, RbmC, or Bap1. These experiments confirmed that *V. cholerae* is indeed producing biofilm matrix in direct proximity to *E. coli* (*SI Appendix*, Fig. S9 *A–C*). We also found, surprisingly, that RbmC localizes substantially above background around *E. coli* cells (*SI Appendix*, Fig. S9 *B* and *D*). This result was supported by experiments in which cell-free *V. cholerae* supernatant containing RbmC-FLAG was added to *E. coli* biofilms growing in monoculture (*SI Appendix*, Fig. S10). RbmC is a diffusible matrix protein that participates in the internal architecture of *V. cholerae* clonal cell groups but also, importantly, contributes to binding of the cell groups to the underlying surface (27, 29, 71). The mechanical details of binding between the group and surface are important for the transition from lateral expansion of flat monolayers to the extension of *V. cholerae* biofilms into 3D space and subsequent packing architecture (29, 81). Accumulation of RbmC around *E. coli* does not appear to diminish the amount of RbmC that *V. cholerae* accumulates around itself relative to monoculture conditions (*SI Appendix*, Fig. S9*E*). Nevertheless, the localization of this matrix protein around *E. coli* in close proximity to *V. cholerae* may potentially contribute to the disruption of normal *V. cholerae* cell group architecture when the two species begin biofilm growth directly adjacent to each other. The precise physical and biochemical details of how multispecies biofilm architecture quantitatively and qualitatively departs from clonal biofilm architecture will be an important area for future work.

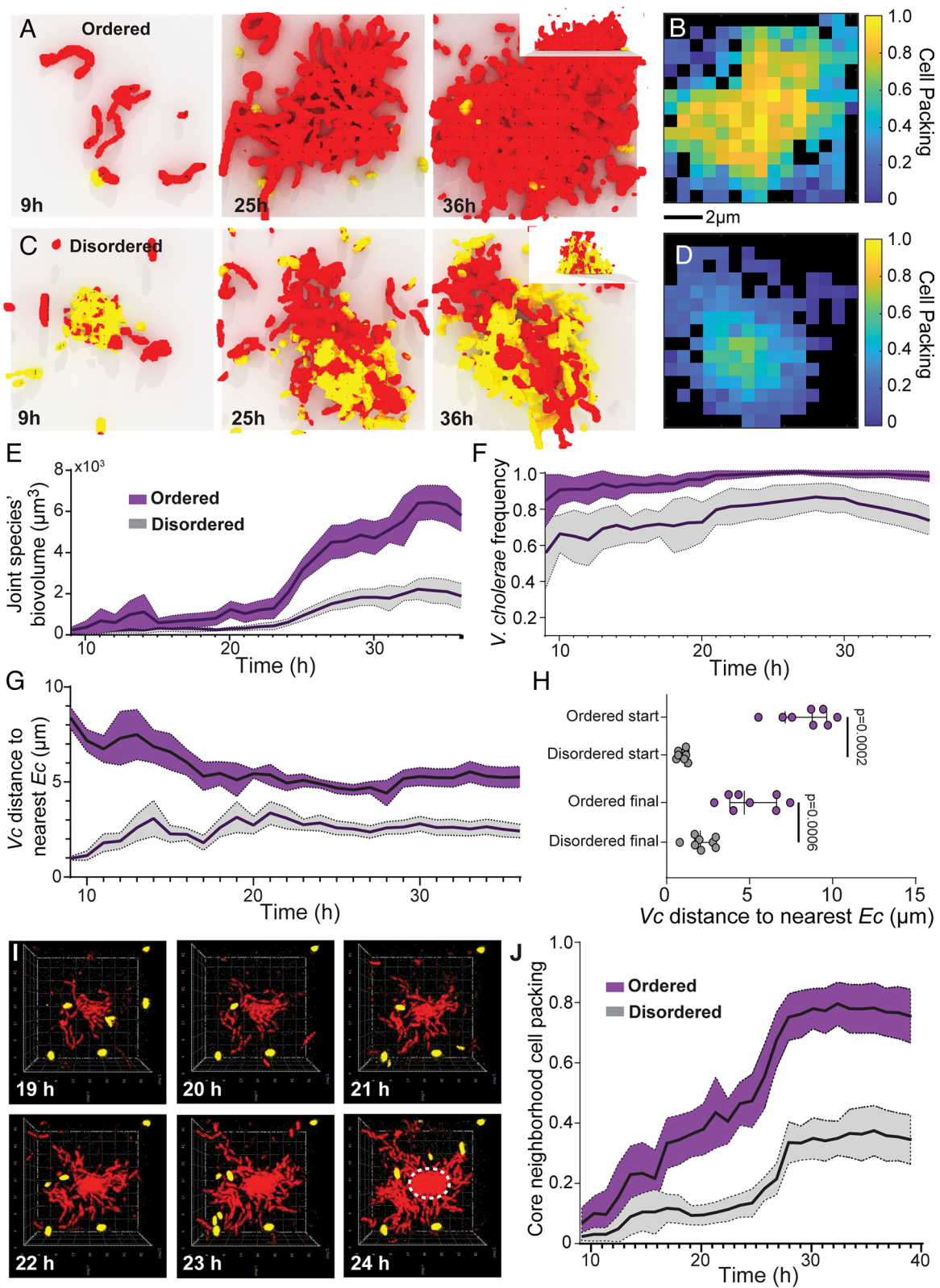


Fig. 4. Initial distance between *V. cholerae* (red) and *E. coli* (yellow) cells best distinguishes colonies that will become highly packed and predation-protected versus disordered and predation-susceptible. (A) Time lapse of 3D renderings of an example ordered cell group with (B) a heatmap for neighborhood cell packing at the 36 h time point. (C) Time lapse of 3D renderings of an example disordered cell group with (D) a heatmap for neighborhood cell packing at the 36 h time point. Renderings in panels A and C are $31 \mu\text{m} \times 31 \mu\text{m} \times 14 \mu\text{m}$ (LxWxD). (E-G) Time courses for (E) combined biovolume of both species, (F) *V. cholerae* frequency, (G) average distance of *V. cholerae* cells to nearest *E. coli* ($n = 8$ for each colony type). (H) Statistical comparison of *V. cholerae* distance to nearest *E. coli* between biofilm types at the start and end of courses in G (Mann-Whitney *U* tests with $n = 8$). (I) Top-down view of a *V. cholerae* cluster as a core high-packing region nucleates (each rendering is $31 \mu\text{m} \times 31 \mu\text{m} \times 14 \mu\text{m}$ (LxWxD)). The secondary biofilm front that forms the boundary of this core high-packing region is denoted with a dotted white circle in the 24 h time point image. (J) Time courses of neighborhood cell packing in the core regions (within 10 μm of colony center) of both colony types ($n = 8$).

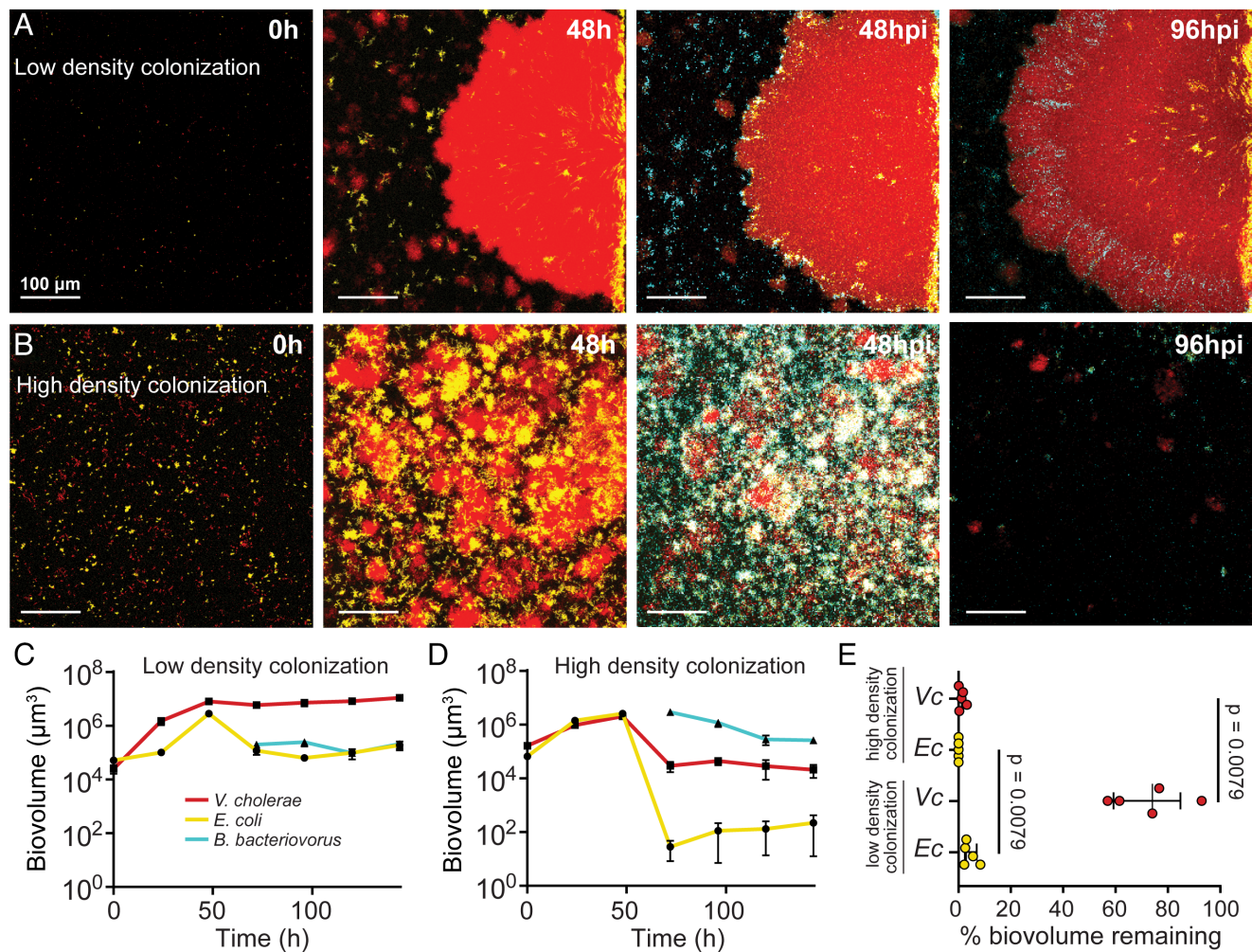


Fig. 5. Initial surface colonization density alters the fraction of highly packed versus disordered colonies of *V. cholerae* (red) and *E. coli* (yellow), which in turn alters overall population dynamics and *B. bacteriovorus* (cyan) predator survival for both prey. (A and B) Representative image sets of the low-density (A) and high-density (B) colonization conditions at initial surface colonization through 96 h post-predator introduction. (C and D) Biovolume of all three species as a proxy for their population dynamics in the (C) low-density initial condition and (D) high-density initial condition ($n = 5$). (E) Percent of each prey species remaining at the end of the predation experiments in the low and high colonization density initial conditions ($n = 5$; plots denote medians with interquartile ranges). The percentage remaining is calculated as the biovolume of each prey species at the last time point (146 h) relative to the biovolume that was present just prior to the introduction of *B. bacteriovorus* predators. Pairwise comparisons denote Mann-Whitney U tests.

Surface Colonization Strongly Impacts Population Dynamics via its Influence on Biofilm Architecture. Our results above suggest that the average distance between *V. cholerae* and *E. coli* cells at the start of biofilm growth should directly determine the relative occurrence of ordered, highly packed *V. cholerae* groups that envelope pockets of surface-attached *E. coli* as they expand, as opposed to disordered dual-species cell groups. As highly packed *V. cholerae* cell groups are protected from *B. bacteriovorus*, while disordered colonies are not, our observations lead to the ecological prediction that initial surface colonization conditions, via their impact on the relative proportion of highly packed versus disordered dual-species colonies, can substantially change the population dynamics of predator-prey interaction. In other words, the initial surface coverage should indirectly determine the overall impact of predation on survival of both species via its direct impact on colony structure development. We tested this prediction by inoculating two sets of two-species chambers with relatively low or high surface colonization density (20% versus 60% surface coverage, respectively, *SI Appendix*, Fig. S11A). Low or high initial density alters the distributions of distance between *V. cholerae* and *E. coli* cells (*SI Appendix*, Fig. S11B), in turn leading to large amounts of highly packed *V. cholerae* colonies containing small numbers of *E. coli* (low initial density), or mostly disordered,

mixed colonies containing more evenly distributed *V. cholerae* and *E. coli* (high initial density) (Fig. 5 A and B).

As anticipated, low versus high initial surface occupation led to distinct survival outcomes for both prey species after the introduction of *B. bacteriovorus*. In the low initial density condition, the majority of *V. cholerae*, as well as the smaller groups of *E. coli* embedded in their packed biofilms, survive predator exposure (Fig. 5 A, C, and E). By contrast, in the high initial density conditions predominated by disordered groups of *V. cholerae* and *E. coli*, a far greater fraction of the dual-species prey community is killed off by *B. bacteriovorus* (Fig. 5 B, D and E). Taken together, these data are consistent with our prediction that surface colonization conditions determine the relative amounts of ordered versus disordered biofilm cell groups of *E. coli* and *V. cholerae*, which in turn govern the survival of both prey species under *B. bacteriovorus* predation.

Discussion

Exploration of multispecies biofilm communities using live high-resolution imaging is crucial to understanding microbial ecology at the spatial scale on which cell-cell interactions occur (11, 20, 23, 82–91). Here we tracked the spatial population dynamics of the

bacterial predator *B. bacteriovorus* in dual-species prey biofilms of *V. cholerae* and *E. coli*, finding that the survival rates of both prey species are altered, but in opposite directions, when they are growing together. *V. cholerae* produces biofilm cell clusters that reach a cell packing density threshold past which *B. bacteriovorus* cannot enter, protecting the prey within. *E. coli* can become enveloped along the basal layers of these highly packed structures, co-opting predator protection from *V. cholerae* and increasing *E. coli* survival relative to when growing on its own. By contrast, in dual-species biofilms, a fraction of *V. cholerae* becomes entangled with *E. coli* early during biofilm growth, leading to an alternate structure that is more homogeneously mixed, disordered, and loosely packed. These disordered cell groups do not block predator cell entry, and all prey within them are killed by *B. bacteriovorus*. As a result of these biofilm structural dynamics, *V. cholerae* survival decreases in co-culture with *E. coli* relative to when growing on its own. At any given location, which of these two alternative cell group structures emerge depends on the initial distance between *V. cholerae* and *E. coli* cells that have attached to the underlying surface. Surface colonization patterns therefore determine the relative occurrence of predation-protected cell groups versus susceptible cell groups and the overall rates of *B. bacteriovorus* predator survival for each prey species.

This study makes explicit that the cellular arrangement and tightly packed structure of clonal *V. cholerae* groups can operate as a type of public good (39, 92) that confers predator protection to the cells within [among many other benefits (30, 33–35, 55, 74, 93–97)]. Other species—here, *E. coli*, whose mono-species biofilms are susceptible to *B. bacteriovorus*—can take advantage of this protective architecture when small groups of them become enveloped by expanding, highly packed biofilms of *V. cholerae*. By contrast, if too many *E. coli* cells are present in close enough proximity to *V. cholerae* at the start of biofilm growth, then *V. cholerae* cannot initiate its normal cell group structure, and the public good benefit of predation protection completely breaks down in that location. It is notable that the spatial architecture of biofilm-producing bacteria can manifest as a public good that is exploitable across species in this manner. In this case, the stability of *V. cholerae* cooperative architecture depends on the initial surface population density, which determines whether *V. cholerae* cell lineages have enough space to nucleate the highly packed core regions of expanding biofilm clusters before encountering cells of other species. Though distinct in mechanistic detail, this example should fall under related social evolution principles as other kinds of microbial cooperation that provide benefits in a distance-dependent manner. Recent work has highlighted in detail how the population dynamics and evolutionary stability of this class of cooperative behavior depend on the spatial range of cooperative sharing, the population/community composition, and spatial cell arrangements during early biofilm growth (33, 34, 39, 93, 96, 98).

The interplay of *V. cholerae*, *E. coli*, and *B. bacteriovorus* in co-culture emphasizes that the population dynamics of different species in a community can depend quite strongly on the cellular resolution details of biofilm structure, which in turn can differ in unexpected ways between mono-species and multispecies systems. In recent years microbiologists have made tremendous strides in understanding the cellular and molecular nuances of biofilm architecture and their relationship to microbial ecology and evolution. By necessity for tractability in many cases, much of this work has focused on one species at a time. Our experiments here highlight how new and interesting questions about the drivers of biofilm structure, and the relationship between biofilm structure and community ecology, can arise from modest increases in complexity with multispecies systems. Here, it appears as though *E. coli*—if adjacent to *V. cholerae* at the start of biofilm growth—may interfere with normal localization of

at least one component of the *V. cholerae* matrix, which could then contribute to the qualitative differences in ordered versus disordered architectures that appear later during biofilm growth.

The connection between initial surface coverage and multispecies prey biofilm architecture, and the additional connection between biofilm architecture and predator exposure, together lead to an interesting dependence between early biofilm growth conditions and predator–prey ecology. It would be fruitful to explore how and when these relationships generalize to other species combinations and biofilm environmental growth conditions with increasing ecological realism. Where prior studies have analyzed multispecies biofilms at high resolution, they have also indicated important consequences for community structure and environmental impacts (11, 12, 22, 47, 48, 99–103). A notable recent example examined the detailed structure of multispecies biofilm communities growing as plaque in dental caries (48). Kim et al. showed that *Streptococcus mutans* forms consistent spatial arrangements in biofilm co-culture with other oral microbiota species. In this case, *S. mutans* consistently produces core clonal regions, around which form layers of non-*mutans* streptococci followed by non-streptococci. The metabolic activity of *S. mutans* within the inner regions of these multispecies biofilms caused low local pH that could recapitulate the rapid demineralization of enamel that occurs during development of caries *in vivo*.

Our work here highlights how the details of early surface colonization conditions can cascade into qualitative differences in subsequent biofilm architecture and ecological dynamics. This result points to several goals for future work. Any phenotypes that alter surface exploration or settling patterns, including gliding and twitching motility, as well as any positive or negative interactions within and between species—for example, via shared adhesin production, metabolite trophic interaction, or toxin secretion—could also cascade to major differences in biofilm spatial architecture. Differences in environmental topography and the orientation of nutrient supply, which may often derive in natural environments from the underlying surface rather surrounding liquid, should also be pursued to gain a fuller picture of how the subtleties of biofilm growth in realistic environments impact community structure. Novel experimental systems that implement these increases in ecological realism while maintaining access by high-resolution imaging will be important platforms for further study.

Materials and Methods

V. cholerae strain N16961, *E. coli* strain AR3110, *B. bacteriovorus* strain 109J, and their fluorescent derivatives were cultivated using standard microbiology techniques. All biofilm experiments were performed with syringe pump-driven microfluidic devices fabricated using polydimethylsiloxane bonded to glass coverslips. Image data were gathered using Zeiss 880 and 980 point-scanning confocal microscopes and analyzed using the freely available BiofilmQ framework (104). A detailed description of all methods is provided in the *SI Appendix, Materials and Methods*.

Data, Materials, and Software Availability. Raw numerical data corresponding to all main text and SI figures are included in *SI Appendix, Data S1*.

ACKNOWLEDGMENTS. We are grateful to Blair Costelloe, Robert Cramer, Matthew Ayres, and Jing Yan for helpful advice on earlier versions of the manuscript, and to members of the Nadell Lab and microbiology community at Dartmouth for their input during development of the project. B.R.W. received support from a Gillman Fellowship from the Dartmouth Department of Biological Sciences. J.B.W. was supported by a GAANN Fellowship from the Dartmouth Department of Biological Sciences. C.D.N. received support from the Simons Foundation award number 826672, NSF grant IOS 2017879, NSF grant MCB 1817352, and grant RGY0077/2020 from the Human Frontier Science Program.

1. E. Mayr, 80 years of watching the evolutionary scenery. *Science* **305**, 46–47 (2004).
2. O. X. Cordero, M. S. Datta, Microbial interactions and community assembly at microscales. *Curr. Opin. Microbiol.* **31**, 227–234 (2016).
3. M. Gralka, R. Szabo, R. Stocker, O. X. Cordero, Trophic interactions and the drivers of microbial community assembly. *Curr. Biol. CB* **30**, R1176–R1188 (2020).
4. M. E. Hibbing, C. Fuqua, M. R. Parsek, S. B. Peterson, Bacterial competition: Surviving and thriving in the microbial jungle. *Nat. Rev. Microbiol.* **8**, 15–25 (2010).
5. M. S. Datta, E. Slivierska, J. Gore, M. F. Polz, O. X. Cordero, Microbial interactions lead to rapid microscale successions on model marine particles. *Nat. Commun.* **7**, 11965–11965 (2016).
6. Y. Yawata *et al.*, Competition-dispersal tradeoff ecologically differentiates recently speciated marine bacterioplankton populations. *Proc. Natl. Acad. Sci. U.S.A.* **111**, 5622–5627 (2014).
7. W.-S. Shu, L.-N. Huang, Microbial diversity in extreme environments. *Nat. Rev. Microbiol.* **20**, 219–235 (2022).
8. J. de Dios Caballero *et al.*, Individual patterns of complexity in cystic fibrosis lung microbiota, including predator bacteria, over a 1-year period. *mBio* **8**, e00959–17 (2017).
9. S. Alavi *et al.*, Interpersonal gut microbiome variation drives susceptibility and resistance to cholera infection. *Cell* **181**, 1533–1546.e13 (2020).
10. R. Wolff, W. Shoemaker, N. Garud, Ecological stability emerges at the level of strains in the human gut microbiome. *bioRxiv* [Preprint] (2021). <https://doi.org/10.1101/2021.09.30.462616> (Accessed 13 December 2022).
11. K. A. Earle *et al.*, Quantitative imaging of gut microbiota spatial organization. *Cell Host Microbe* **18**, 478–488 (2015).
12. J. L. Mark Welch, Y. Hasegawa, N. P. McNulty, J. I. Gordon, G. G. Boris, Spatial organization of a model 15-member human gut microbiota established in gnotobiotic mice. *Proc. Natl. Acad. Sci. U.S.A.* **114**, E9105–E9114 (2017).
13. N. S. Jakubovics, S. D. Goodman, L. Mashburn-Warren, G. P. Stafford, F. Cieplik, The dental plaque biofilm matrix. *Periodontol 2000* **86**, 32–56 (2021).
14. P. D. Marsh, Dental plaque as a biofilm and a microbial community – Implications for health and disease. *BMC Oral Health* **6**, S14 (2006).
15. L. R. Frost, J. K. J. Cheng, M. Unnikrishnan, Clostridioides difficile biofilms: A mechanism of persistence in the gut? *PLOS Pathog.* **17**, e1009348 (2021).
16. N. Béchon, J.-M. Ghigo, Gut biofilms: Bacteroides as model symbionts to study biofilm formation by intestinal anaerobes. *FEMS Microbiol. Rev.* **46**, fuab054 (2022).
17. H.-C. Flemming, Biofouling in water systems – cases, causes and countermeasures. *Appl. Microbiol. Biotechnol.* **59**, 629–640 (2002).
18. H. Huang *et al.*, Towards the biofilm characterization and regulation in biological wastewater treatment. *Appl. Microbiol. Biotechnol.* **103**, 1115–1129 (2019).
19. J. P. Boltz *et al.*, From biofilm ecology to reactors: A focused review. *Water Sci. Technol. J. Int. Assoc. Water Pollut. Res.* **75**, 1753–1760 (2017).
20. M. Burmølle, L. H. Hansen, S. J. Sørensen, Establishment and early succession of a multispecies biofilm composed of soil bacteria. *Microb. Ecol.* **54**, 352–362 (2007).
21. H. Dang, C. R. Lovell, Microbial surface colonization and biofilm development in marine environments. *Microbiol. Mol. Biol. Rev. MMBR* **80**, 91–138 (2016).
22. G. E. Leventhal *et al.*, Strain-level diversity drives alternative community types in millimetre-scale granular biofilms. *Nat. Microbiol.* **3**, 1295–1303 (2018).
23. S. Mitri, J. B. Xavier, K. R. Foster, Social evolution in multispecies biofilms. *Proc. Natl. Acad. Sci. U.S.A.* **108**, 10839–10846 (2011).
24. D. Rao, J. S. Webb, S. Kjelleberg, Competitive interactions in mixed-species biofilms containing the marine bacterium *Pseudoalteromonas tunicata*. *Appl. Environ. Microbiol.* **71**, 1729–36 (2005).
25. B. R. Wucher *et al.*, *Vibrio cholerae* filamentation promotes chitin surface attachment at the expense of competition in biofilms. *Proc. Natl. Acad. Sci. U.S.A.* **116**, 14216–14221 (2019).
26. C. Absalon, K. Van Dellen, P. I. Watnick, A communal bacterial adhesin anchors biofilm and bystander cells to surfaces. *PLoS Pathog.* **7**, e1002210–e1002210 (2011).
27. V. Berk *et al.*, Molecular architecture and assembly principles of *Vibrio cholerae* biofilms. *Science* **337**, 236–239 (2012).
28. K. Drescher *et al.*, Architectural transitions in *Vibrio cholerae* biofilms at single-cell resolution. *Proc. Natl. Acad. Sci. U.S.A.* **113**, E2060–E2072 (2016).
29. J. Yan, A. G. Sharo, H. A. Stone, N. S. Wingreen, B. L. Bassler, *Vibrio cholerae* biofilm growth program and architecture revealed by single-cell live imaging. *Proc. Natl. Acad. Sci. U.S.A.* **113**, E5337–E5343 (2016).
30. J.-S.B. Tai *et al.*, Social evolution of shared biofilm matrix components. *Proc. Natl. Acad. Sci. U.S.A.* **119**, e2123469119 (2022).
31. L. Ma *et al.*, Assembly and development of the *Pseudomonas aeruginosa* biofilm matrix. *PLOS Pathog.* **5**, e1000354 (2009).
32. C. Reichhardt, M. R. Parsek, Confocal laser scanning microscopy for analysis of *Pseudomonas aeruginosa* biofilm architecture and matrix localization. *Front. Microbiol.* **10**, 677 (2019).
33. K. Drescher, C. D. Nadell, H. A. Stone, N. S. Wingreen, B. L. Bassler, Solutions to the public goods dilemma in bacterial biofilms. *Curr. Biol.* **24**, 50–55 (2014).
34. C. D. Nadell, K. Drescher, N. S. Wingreen, B. L. Bassler, Extracellular matrix structure governs invasion resistance in bacterial biofilms. *ISME J.* **9**, 1700–1709 (2015).
35. B. R. Wucher, M. Elsayed, J. S. Adelman, D. E. Kadouri, C. D. Nadell, Bacterial predation transforms the landscape and community assembly of biofilms. *Curr. Biol. CB* **31**, 2643–2651.e3 (2021).
36. D. Kadouri, G. A. O'Toole, Susceptibility of biofilms to *Bdellovibrio* bacteriovorus attack. *Appl. Environ. Microbiol.* **71**, 4044–4051 (2005).
37. F. Díaz-Pascual *et al.*, Breakdown of *Vibrio cholerae* biofilm architecture induced by antibiotics disrupts community barrier function. *Nat. Microbiol.* **4**, 2136–2145 (2019).
38. C. D. Nadell, B. L. Bassler, A fitness trade-off between local competition and dispersal in *Vibrio cholerae* biofilms. *Proc. Natl. Acad. Sci. U.S.A.* **108**, 14181–14185 (2011).
39. C. D. Nadell, K. Drescher, K. R. Foster, Spatial structure, cooperation and competition in biofilms. *Nat. Rev. Microbiol.* **14**, 589–600 (2016).
40. K. M. Giglio, J. C. Fong, F. H. Yildiz, H. Sondermann, Structural basis for biofilm formation via the *Vibrio cholerae* matrix protein RbmA. *J. Bacteriol.* **195**, 3277–3286 (2013).
41. C. D. Nadell, J. B. Xavier, K. R. Foster, The sociobiology of biofilms. *FEMS Microbiol. Rev.* **33**, 206–224 (2009).
42. S. Arnaouteli, N. C. Bamford, N. R. Stanley-Wall, Á.T. Kovács, *Bacillus subtilis* biofilm formation and social interactions. *Nat. Rev. Microbiol.* **19**, 600–614 (2021).
43. T. Abe, Á. T. Kovács, O. P. Kuipers, S. van der Veen, Biofilm formation and dispersal in Gram-positive bacteria. *Curr. Opin. Biotechnol.* **22**, 172–179 (2011).
44. B. Maier, G. C. L. Wong, How bacteria use type IV Pili machinery on surfaces. *Trends Microbiol.* **23**, 775–788 (2015).
45. E. R. Oldewurtel, N. Kouzel, L. Dewenter, K. Henseler, B. Maier, Differential interaction forces govern bacterial sorting in early biofilms. *eLife* **4**, e10811 (2015).
46. C. Reichhardt, C. Wong, D. Passos da Silva, D. J. Wozniak, M. R. Parsek, CdrA interactions within the *Pseudomonas aeruginosa* biofilm matrix safeguard it from proteolysis and promote cellular packing. *mBio* **9**, e01376–18 (2018).
47. J. L. Mark Welch, B. J. Rossetti, C. W. Rieken, F. E. Dewhurst, G. G. Boris, Biogeography of a human oral microbiome at the micron scale. *Proc. Natl. Acad. Sci. U.S.A.* **113**, E791–E800 (2016).
48. D. Kim *et al.*, Spatial mapping of polymicrobial communities reveals a precise biogeography associated with human dental caries. *Proc. Natl. Acad. Sci. U.S.A.* **117**, 12375–12386 (2020).
49. O. Mondragón-Palomino *et al.*, Three-dimensional imaging for the quantification of spatial patterns in microbiota of the intestinal mucosa. *Proc. Natl. Acad. Sci. U.S.A.* **119**, e2118483119 (2022).
50. J. G. Lopez, N. S. Wingreen, Noisy metabolism can promote microbial cross-feeding. *eLife* **11**, e70694 (2022).
51. F. Diaz-Pascual *et al.*, Spatial alanine metabolism determines local growth dynamics of *Escherichia coli* colonies. *eLife* **10**, e70794 (2021).
52. N. C. Drebes Dörr, M. Blokesch, Bacterial type VI secretion system facilitates niche domination. *Proc. Natl. Acad. Sci. U.S.A.* **115**, 8855–8857 (2018).
53. W. P. J. Smith *et al.*, The evolution of tit-for-tat in bacteria via the type VI secretion system. *Nat. Commun.* **11**, 5395 (2020).
54. E. T. Granato, T. A. Meiller-Legrand, K. R. Foster, The evolution and ecology of bacterial warfare. *Curr. Biol. CB* **29**, R521–R537 (2019).
55. B. S. Tseng *et al.*, The extracellular matrix protects *Pseudomonas aeruginosa* biofilms by limiting the penetration of tobramycin. *Environ. Microbiol.* **15**, 2865–2878 (2013).
56. Y. Wang *et al.*, Mouse model of hemogenous implant-related *Staphylococcus aureus* biofilm infection reveals therapeutic targets. *Proc. Natl. Acad. Sci. U.S.A.* **114**, E5094–E5102 (2017).
57. A. Dashoff, R. A. Junka, M. Libera, D. E. Kadouri, Predation of human pathogens by the predatory bacteria *Micavibrio aeruginosavorus* and *Bdellovibrio bacteriovorus*. *J. Appl. Microbiol.* **110**, 431–444 (2011).
58. S. Otto, E. P. Bruni, H. Harms, L. Y. Wick, Catch me if you can: Dispersal and foraging of *Bdellovibrio bacteriovorus* 109 J along mycelia. *ISME J.* **11**, 386–393 (2017).
59. R. E. Sockett, Predatory lifestyle of *Bdellovibrio bacteriovorus*. *Annu. Rev. Microbiol.* **63**, 523–539 (2009).
60. J. K. Summers, J.-U. Kreft, Predation strategies of the bacterium *Bdellovibrio bacteriovorus* result in overexploitation and bottlenecks. *Appl. Environ. Microbiol.* **88**, e010821 (2022).
61. K. J. Evans, C. Lambert, R. E. Sockett, Predation by *Bdellovibrio bacteriovorus* HD100 requires type IV pili. *J. Bacteriol.* **189**, 4850–4859 (2007).
62. M. C. Duncan *et al.*, High-throughput analysis of gene function in the bacterial predator *Bdellovibrio bacteriovorus*. *mBio* **10**, e01040–19 (2019).
63. V. lebba *et al.*, *Bdellovibrio bacteriovorus* directly attacks *Pseudomonas aeruginosa* and *Staphylococcus aureus* Cystic fibrosis isolates. *Front. Microbiol.* **5**, 280 (2014).
64. O. Gorenlik *et al.*, *Vibrio cholerae* autoinducer-1 enhances the virulence of enteropathogenic *Escherichia coli*. *Sci. Rep.* **9**, 4122 (2019).
65. C. Abriat *et al.*, Mechanical and microstructural insights of *Vibrio cholerae* and *Escherichia coli* dual-species biofilm at the air-liquid interface. *Colloids Surf. B Biointerfaces* **188**, 110786 (2020).
66. S. Chakraborty *et al.*, Concomitant infection of enterotoxigenic *Escherichia coli* in an outbreak of cholera caused by *Vibrio cholerae* O1 and O139 in Ahmedabad, India. *J. Clin. Microbiol.* **39**, 3241–3246 (2001).
67. M. A. Hood, G. E. Ness, Survival of *Vibrio cholerae* and *Escherichia coli* in estuarine waters and sediments. *Appl. Environ. Microbiol.* **43**, 578–584 (1982).
68. H. Wang, Contributions of *Escherichia coli* and its motility to the formation of dual-species biofilms with *Vibrio cholerae*. *Appl. Environ. Microbiol.* **87**, e00938–21 (2021).
69. N. J. Shikuma, M. G. Hadfield, Marine biofilms on submerged surfaces are a reservoir for *Escherichia coli* and *Vibrio cholerae*. *Biofouling* **26**, 39–46 (2010).
70. F. H. Yıldız, K. L. Visick, *Vibrio* biofilms: So much the same yet so different. *Trends Microbiol.* **17**, 109–118 (2009).
71. J. K. Teschler, C. D. Nadell, K. Drescher, F. H. Yıldız, Mechanisms underlying *Vibrio cholerae* biofilm formation and dispersion. *Annu. Rev. Microbiol.* **76**, 503–532 (2022).
72. J. K. Teschler *et al.*, Living in the matrix: Assembly and control of *Vibrio cholerae* biofilms. *Nat. Rev. Microbiol.* **13**, 255–268 (2015).
73. D. O. Serra, R. Hengge, Bacterial multicellularity: The biology of *Escherichia coli* building large-scale biofilm communities. *Annu. Rev. Microbiol.* **75**, 269–290 (2021).
74. L. Vidakovic, P. K. Singh, R. Hartmann, C. D. Nadell, K. Drescher, Dynamic biofilm architecture confers individual and collective mechanisms of viral protection. *Nat. Microbiol.* **3**, 26–31 (2018).
75. V. Bachmann *et al.*, Bile salts modulate the mucin-activated type VI secretion system of pandemic *Vibrio cholerae*. *PLoS Negl. Trop. Dis.* **9**, e0004031 (2015).
76. D. L. MacIntyre, S. T. Miyata, M. Kitaoka, S. Pukatzki, The *Vibrio cholerae* type VI secretion system displays antimicrobial properties. *Proc. Natl. Acad. Sci. U.S.A.* **107**, 19520–19524 (2010).
77. E. E. Bernardy, M. A. Turnsek, S. K. Wilson, C. L. Tarr, B. K. Hammer, Diversity of clinical and environmental isolates of *Vibrio cholerae* in natural transformation and contact-dependent bacterial killing indicative of type VI secretion system activity. *Appl. Environ. Microbiol.* **82**, 2833–2842 (2016).
78. J. B. Winans, B. R. Wucher, C. D. Nadell, Cell group architecture dictates phage exposure in multispecies biofilms. *PLOS Biol* **20**, e3001913 (2022).
79. R. Hartmann *et al.*, Emergence of three-dimensional order and structure in growing biofilms. *Nat. Phys.* **15**, 251–256 (2019).
80. Qin *et al.*, Cell position fates and collective fountain flow in bacterial biofilms revealed by light-sheet microscopy. *Science* **369**, 71–77 (2020).
81. J. Nijjer *et al.*, Mechanical forces drive a reorientation cascade leading to biofilm self-patterning. *Nat. Commun.* **12**, 6632 (2021).
82. M. R. Parsek, E. P. Greenberg, Sociomicrobiology: The connections between quorum sensing and biofilms. *Trends Microbiol.* **13**, 27–33 (2005).
83. S. Mitri, E. Clarke, K. R. Foster, Resource limitation drives spatial organization in microbial groups. *ISME J.* **10**, 1471–1482 (2016).

84. M. Ghoul, S. Mitri, The ecology and evolution of microbial competition. *Trends Microbiol.* **24**, 833–845 (2016).
85. P. Piccardi, B. Vessman, S. Mitri, Toxicity drives facilitation between 4 bacterial species. *Proc. Natl. Acad. Sci. U.S.A.* **116**, 15979–15984 (2019).
86. K. Z. Coyle, J. Schlüter, K. R. Foster, The ecology of the microbiome: Networks, competition, and stability. *Science* **350**, 663–666 (2015).
87. S. E. Darch, S. A. West, K. Winzer, S. P. Diggle, Density-dependent fitness benefits in quorum-sensing bacterial populations. *Proc. Natl. Acad. Sci. U.S.A.* **109**, 8259–8263 (2012).
88. A. Stacy, L. McNally, S. E. Darch, S. P. Brown, M. Whiteley, The biogeography of polymicrobial infection. *Nat. Rev. Microbiol.* **14**, 93–105 (2016).
89. H. M. Kurkjian, M. J. Akbari, B. Momeni, The impact of interactions on invasion and colonization resistance in microbial communities. *PLoS Comput. Biol.* **17**, e1008643 (2021).
90. B. Momeni, A. J. Waite, W. Shou, Spatial self-organization favors heterotypic cooperation over cheating. *eLife* **2**, e00960 (2013).
91. S. Widder *et al.*, Challenges in microbial ecology: Building predictive understanding of community function and dynamics. *ISME J.* **10**, 2557–2568 (2016).
92. F. Dionisio, I. Gordo, The tragedy of the commons, the public goods dilemma, and the meaning of rivalry and excludability in evolutionary biology. *Evol. Ecol. Res.* **8**, 321–332 (2006).
93. A. Ebrahimi, J. Schwartzman, O. X. Cordero, Cooperation and spatial self-organization determine rate and efficiency of particulate organic matter degradation in marine bacteria. *Proc. Natl. Acad. Sci.* **116**, 23309–23316 (2019).
94. J. A. Schwartzman, Bacterial growth in multicellular aggregates leads to the emergence of complex lifecycles. *bioRxiv* [Preprint] (2021). <https://doi.org/10.1101/2021.11.01.466752> (Accessed 1 November 2021).
95. J. van Gestel, F. J. Weissing, O. P. Kuipers, Á. T. Kovács, Density of founder cells affects spatial pattern formation and cooperation in *Bacillus subtilis* biofilms. *ISME J.* **8**, 2069–2079 (2014).
96. A. Dragóš *et al.*, Division of labor during biofilm matrix production. *Curr. Biol.* **28**, 1903–1913.e5 (2018).
97. T. Jautzus, J. van Gestel, Á. T. Kovács, Complex extracellular biology drives surface competition during colony expansion in *Bacillus subtilis*. *ISME J.* **16**, 1–9 (2022).
98. J. A. Danone, J. Gore, Understanding microbial cooperation. *J. Theor. Biol.* **299**, 31–41 (2012).
99. C. H. Tan, K. W. K. Lee, M. Burmølle, S. Kjelleberg, S. A. Rice, All together now: Experimental multispecies biofilm model systems. *Environ. Microbiol.* **19**, 42–53 (2017).
100. H. L. Röder, N. M. C. Olsen, M. Whiteley, M. Burmølle, Unravelling interspecies interactions across heterogeneities in complex biofilm communities. *Environ. Microbiol.* **22**, 5–16 (2020).
101. T. N. Enke, G. E. Leventhal, M. Metzger, J. T. Saavedra, O. X. Cordero, Microscale ecology regulates particulate organic matter turnover in model marine microbial communities. *Nat. Commun.* **9**, 2743 (2018).
102. B. E. Wolfe, J. E. Button, M. Santarelli, R. J. Dutton, Cheese rind communities provide tractable systems for *in situ* and *in vitro* studies of microbial diversity. *Cell* **158**, 422–433 (2014).
103. S. A. Huws, A. J. McBain, P. Gilbert, Protozoan grazing and its impact upon population dynamics in biofilm communities. *J. Appl. Microbiol.* **98**, 238–244 (2005).
104. R. Hartmann *et al.*, Quantitative image analysis of microbial communities with BiofilmQ. *Nat. Microbiol.* **6**, 151–156 (2021).